Manufacturing and Characterization of Green Composites with Partially Biobased Epoxy Resin and Flaxseed Flour Wastes

Diego Lascano [1,2] **, Daniel Garcia-Garcia** [1,*] **, Sandra Rojas-Lema** [1,2] **, Luis Quiles-Carrillo** [1] **, Rafael Balart** [1] **and Teodomiro Boronat** [1]

[1] Technological Institute of Materials (ITM), Universitat Politècnica de València (UPV), Plaza Ferrándiz y Carbonell 1, 03801 Alcoy, Spain; dielas@epsa.upv.es (D.L.); sanrole@epsa.upv.es (S.R.-L.); luiquic1@epsa.upv.es (L.Q.-C.); rbalart@mcm.upv.es (R.B.); tboronat@dimm.upv.es (T.B.)

[2] Escuela Politécnica Nacional, Quito 17-01-2759, Ecuador

* Correspondence: dagarga4@epsa.upv.es; Tel.: +(34)96-652-84-34

check for updates

Featured Application: In the present work, green-composites have been developed from a partially biobased epoxy resin reinforced with flaxseed flour wastes. The attractive aesthetic appearance, similar to wood, and the balanced overall properties of the obtained composites may be interesting for use in sectors such as decoration, furniture or automotive industry.

Abstract: In the present work, green-composites from a partially biobased epoxy resin (BioEP) reinforced with lignocellulosic particles, obtained from flax industry by-products or wastes, have been manufactured by casting. In this study, the flaxseed has been crushed by two different mechanical milling processes to achieve different particle sizes, namely coarse size (CFF), and fine size (FFF) particle flaxseed flour, with a particle size ranging between 100–220 μm and 40–140 μm respectively. Subsequently, different loadings of each particle size (10, 20, 30, and 40 wt%) were mixed with the BioEP resin and poured into a mold and subjected to a curing cycle to obtain solid samples for mechanical, thermal, water absorption, and morphological characterization. The main aim of this research was to study the effect of the particle size and its content on the overall properties of composites with BioEP. The results show that the best mechanical properties were obtained for composites with a low reinforcement content (10 wt%) and with the finest particle size (FFF) due to a better dispersion into the matrix, and a better polymer-particle interaction too. This also resulted in a lower water absorption capacity due to the presence of fewer voids in the developed composites. Therefore, this study shows the feasibility of using flax wastes from the seeds as a filler in highly environmentally friendly composites with a wood-like appearance with potential use in furniture or automotive sectors.

1. Introduction

During the last years, there has been a significant increase in social concern for the environmental problem generated by petrochemical polymeric materials [1–3]. For this reason, one of the main objectives of the scientific community is the research and development of new highly environmentally friendly materials which could be suitable to replace petroleum-based polymers to reduce their carbon footprint [4]. Many of these researches focus on the field of polymer composites reinforced with lignocellulosic particles giving rise to the so-called wood plastic composites (WPC). A series of advantages make the use of lignocellulosic reinforcements very attractive for their use as reinforcement,

such as their low cost, low density, non-abrasive properties, non-toxic, biodegradable, and their environmentally friendly nature [5,6]. Besides, the lignocellulosic particles usually provide an aesthetic wood-like surface finish, which makes them very interesting for use in sectors where aesthetics is an essential factor, such as the furniture or automotive sectors. Furthermore, WPCs have several advantages over wood, such as low maintenance, high dimensional stability, and high resistance to biological attack [7,8]. There are many research works that have focused on the effect of different types of lignocellulosic particles on the properties of both thermoplastic and thermoset matrices. For example, interesting works have been developed with rice husks [9–11], peanut shells [7,12,13], almond shells [14–16], hazelnut shells [17,18], date palm seeds [19], lemon peel [20], *Posidonia oceanica* [21,22], olive stones [23], among others. Most of these lignocellulosic particles come from agricultural by-products or wastes that are currently used for animal feeding and just left on controlled landfills. Therefore, the use of these wastes, widely available as a source of fillers for composite materials, can be a new economic opportunity for the agricultural sector and thereby contributing to generate sustainable circular economies [24–26].

Flax (*Linum usitatissimum L.*) is a worldwide cultivated plant, mainly for obtaining fibers and oil-rich seeds [27]. It is estimated that the world production of flaxseed, also known as linseed, was approximately 3.2 million tons during 2018 [28]. Traditionally flaxseeds have been used as an oil source, due to its high triglyceride content (between 30 and 41 wt%), for use in paints and coatings, linoleum, inks, varnishes, cosmetics, soap production, among others [29,30]. However, over the past few years, the flaxseed oil has also gained popularity as a nutritional supplement due to its high content of α-linolenic acid (ALA), an omega-3 fatty acid beneficial in preventing cardiovascular disease or hypertension [31]. In addition, many studies have shown that flaxseed oil has a positive effect on diseases such as hyperlipidaemia, colon and breast cancer, or atherosclerosis [32]. The main by-product generated during oil extraction is flaxseed cake, which is the solid mass left after the seeds are pressed during the oil extraction process. For this reason, flaxseed cake is widely available and, a cost-effective and environmentally friendly material to be used in composites [33]. The flaxseed cake is rich in cyanogenic glycosides, which may be degraded to toxic hydrogen cyanide (HCN) upon ingestion and may represent a risk to human health if used in food applications without prior detoxification treatment [31]. For this reason, currently, a part of this by-product is spray-dried to obtain flour (flaxseed flour), which is used as a low-value by-product for obtaining livestock feed or fertilizers [34,35]. In other cases, this waste is used for composting or simply incinerated [36]. Therefore, the flaxseed flour can potentially be a candidate for use in composites.

Furthermore, a significant part of the plastic matrices used in WPCs is thermoplastic petroleum-derived polymers such as polypropylene (PP), polyethylene (PE), polystyrene (PS), polyvinylchloride (PVC), among others. However, there has been a tendency in recent years to replace these matrices by biobased and biodegradable (actually soil compostable) polymers such as polylactic acid (PLA) or polyhydroxyalkanoates (PHA) [37], to achieve fully biodegradable WPCs. Natural fiber reinforced plastics (NFRP) represent a wider group that includes WPCs and thermosetting-based composites, as well. For thermosetting resins, this trend is focused on the use of fully or partially biobased resins [38–42]. With this, it is possible to reduce the dependence on fossil fuels. Besides this, these fully/partially thermosetting resins, positively contribute to reducing the carbon footprint generated by their petrochemical counterparts such as phenolics (PF), epoxies (EP), or unsaturated polyesters (UP). A promising source for biobased epoxy resins and plasticizers are epoxidized vegetable oils, which are obtained by epoxidizing the C-C double bonds of unsaturated fatty acids contained in triglycerides, the main component of vegetable oils [43–45]. However, due to the long aliphatic chains in the triglycerides and their low cross-linking density, epoxy resins obtained from vegetable oils tend to have low glass transition temperatures (T_g) and lower mechanical properties than traditional epoxy resins [46]. Therefore, to obtain environmentally friendly materials with balanced mechanical and thermal properties, one of the most efficient approaches is copolymerization of epoxidized vegetable oils with petroleum-derived epoxy resins, thus giving rise to a partially biobased epoxy resin with

high mechanical properties [47]. Niedermann et al. [48] investigated the effect of the epoxidized soybean oil (ESO) content (0, 25, 50, 75, and 100 wt%) on bisphenol-A based aromatic epoxy resin (DGEBA). The results showed a decrease in T_g as the ESO content increased but indicated that T_g of the DGEBA/ESO system (75/25) was very similar (138 °C) to the base DGEBA resin (140 °C). Obviously, this was remarkably higher than the T_g of neat crosslinked ESO (75 °C). Similar trends were also observed for mechanical properties such as tensile strength and impact energy, where the addition of 25 wt% ESO decreased the mechanical properties of DGEBA resin but made them more resistant than ESO resin. Regarding the manufacturing of materials with these cast resins, Wu et al. [49] reported impregnation bamboo with epoxy with previous delignification processes to obtain almost transparent bamboo goods. Salasinska et al. [50], reported new environmentally friendly composites with epoxy resins and *Pinus sibirica* lignocellulosic fillers at a constant wt% of 20%. These composites were manufactured at a laboratory scale by mixing the components and finally, a conventional cast method was used to pour the liquid mixture into a mold. Casting is the most widely used method to manufacture composites with thermosetting resins and lignocellulosic particles. Kumar et al. [51] reported manufacturing by casting and characterization of epoxy composites with up to 12.5 wt% wood particles. Centrifugal casting is a way to obtain gradation of the filler due to centrifugal forces as reported by Stabik et al. [52]. They report that as well as the particle gradation occurs, gradation of properties occurs too which could be interesting from different standpoints (decorative, percolation thresholds in some parts, and so on.

The main objective of the present work was to obtain green composites from a partially biobased epoxy resin reinforced with flaxseed flour waste using the casting method. Specifically, the effect of particle size and the content of flaxseed flour on the mechanical, morphological, thermal, and water absorption properties of the bioepoxy/flaxseed flour composites, has been investigated. In the present work, four compositions (10, 20, 30, and 40 wt%) and two-particle sizes (CFF and FFF) were investigated.

2. Materials and Methods

2.1. Materials

The matrix material used in this study was a commercial epoxy resin Resoltech® 1070 ECO (viscosity of 1750 mPa s and a density of 1.18 g cm^{-3} at 23 °C). The hardener was an amine-based system Resoltech® 1074 ECO (viscosity of 50 mPa s and density of 0.96 g cm^{-3} at 23 °C). Both were supplied by Castro Composites (Pontevedra, Spain). The epoxy resin was based on a mixture of a diglycidyl ether of bisphenol A (DGEBA) and a plant-based epoxy reactive diluent from vegetable oil epoxidation. The resin to hardener weight ratio was 100:35 (parts by weight), and as indicated by the supplier the cured resin contained 31 wt% biobased content (according to ASTM D6866-12).

Flaxseed (FS) used in this work was supplied by Sorribas S.A. (Polinyà, Spain). The raw FS was crushed in a grinder (Moulinex, Allençon, France) to obtain flaxseed flour (FF) with an average particle size of 157 μm (CFF–coarse flaxseed flour). Then, a part of the obtained CFF was ground using an ultra-centrifugal mill from Retsch Gmbh model Mill ZM 1000 (Haan, Germany) with a sieve of 250 μm and a rotating speed of 10,000 rpm, obtaining FF with an average particle size of 91 μm (FFF—fine flaxseed flour). Figure 1 shows an image of the raw FS and the obtained FF after each of the grinding processes.

Figure 1. Images corresponding to (**a**) raw flaxseeds (FS); (**b**) flaxseed flour (FF) obtained by grinder (CFF); (**c**) flaxseed flour (FF) obtained by ultracentrifuge (FFF).

2.2. BioEP/FF Composites' Manufacturing

Different contents (10, 20, 30, and 40 wt%) of CFF and FFF were added to the liquid epoxy resin Resoltech® 1070 ECO and were mixed at room temperature in a planetary mixer KAPL 5KPM5 from KitchenAid (Benton Harbor, MI, USA) with a total volume of 4.8 L. First, the FF was added to the mixer with the biobased resin and was subjected to initial homogenization at 40 rpm for 5 min. Then, Resoltech® 1074 ECO hardener was added in the stoichiometric ratio (100:35 wt/wt) to the BioEP/FF mixture and subjected to a second mixing cycle at 60 rpm for 2.5 min. After this two-stage mixing cycle, the resin was subjected to vacuum to remove air bubbles in a vacuum chamber MCP 00ILC from HEK-GmbH (Lubeck, Germany) for 5 min. A maximum vacuum of −1 bar was applied. The resulting resin-filler mixture was poured into a silicone mold designed with standardized cavities for mechanical characterization and then subjected to a curing cycle in an oven at 80 °C for 1 h. Cured samples were post-cured at 150 °C for 30 min. The optimal curing and post-curing conditions of the partially biobased epoxy resin were selected according to a previous study [53]. Finally, cured samples were demolded from the silicone molds and used for different characterizations.

The nomenclature of the samples is denoted with the acronym BioEP_iCFF for samples with FF obtained by a simple grinding process, and BioEP_iFFF for samples reinforced with FF obtained by using an ultra-centrifugal mill, where *i* represents the filler content (10, 20, 30 and 40 wt%).

2.3. BioEP/FF Composites' Characterization

2.3.1. Mechanical Properties

Flexural properties of BioEP resin and BioEP/FF composites were obtained at room temperature in a universal test machine Ibertest ELIB 30 (S.A.E. Ibertest, Madrid, Spain) equipped with a 5 kN load cell following the guidelines of the ISO 178. Rectangular samples with dimensions $80 \times 40 \times 4$ mm^3 were subjected to a three-point bending flexural test with a crosshead speed of 5 mm min^{-1}. At least five specimens of each composition were tested, and characteristic average values were calculated.

Impact-absorbed energy of different samples was obtained in a 1-J Charpy's impact pendulum from Metrotec S.A. (San Sebastián, Spain) as indicated in ISO 179:1993. The values of the impact-absorbed energy of each sample were calculated as the average of the energies obtained for five different specimens.

Shore D hardness values of BioEP resin and BioEP/FF composites were obtained with a Shore D hardness durometer model 676-D from J. Bot Instruments S.A. (Barcelona, Spain) according to ISO 868. At least five different measurements were taken at room temperature, and average values were calculated.

2.3.2. Thermal Properties

Thermal stability at elevated temperatures of BioEP and BioEP/FF composites was studied by thermogravimetric analysis (TGA) using a TGA/SDT 851 thermobalance from Mettler-Toledo Inc. (Schwerzenbach, Switzerland). Samples with an average weight ranging from 7 to 9 mg were heated from 30 to 700 °C at a constant heating rate of 10 °C min^{-1}. All samples were tested in triplicate in a nitrogen atmosphere with a constant nitrogen flow rate of 66 mL min^{-1}. The onset degradation temperature (T_0) was assumed at a weight loss of 5 wt%, and the maximum degradation rate temperature ($T_{\max}$) was obtained as the corresponding peak in the first derivative from TGA curves (DTG).

2.3.3. Thermo-Mechanical Properties

Dynamic mechanical thermal analysis (DMTA) of BioEP and BioEP/FF composites was carried out in torsion mode in an oscillatory rheometer AR G2 by TA Instruments (New Castle, DE, USA) equipped with a special clamp system for solid samples working in a combination of torsion and shear. Rectangular samples ($40 \times 10 \times 4$ mm^3) were subjected to a temperature sweep program from 30 °C to 140 °C at a constant heating rate of 2 °C min^{-1}. The frequency of the dynamic stress was set to 1 Hz, and a maximum shear strain (γ) of 0.1% was used in all tests. The evolution of the storage modulus (G′) and the dynamic damping factor (*tan δ*) were recorded as a function of increasing temperature.

The effect of temperature on the dimensional stability of BioEP/FF composites was studied by thermomechanical analysis (TMA) using a Q400 TMA analyzer from TA Instruments (New Castle, DE, USA). Samples with dimensions of $4 \times 10 \times 10$ mm^3 were subjected to a heating ramp from 0 °C to 140 °C, at a constant heating rate of 2 °C min^{-1}, with an applied load of 20 mN. The coefficient of linear thermal expansion (CLTE) was calculated as the slope of the linear relationship between the expansion and temperature, both below and above T_g. All measurements were done in triplicate to obtain reliable values.

2.3.4. Morphological Properties

The morphology of fractured surfaces from an impact test of BioEP resin, different BioEP/FF composites, and flaxseed flour particles was observed using a field emission scanning electron microscope (FESEM) ZEISS model ULTRA55 (Eindhoven, The Netherlands) working at an acceleration voltage of 2 kV. Before the morphological characterization, all samples were surface coated with a thin layer of platinum in a high vacuum sputter coater EM MED20 from Leica Microsystems (Milton Keynes, UK) to provide electrical conductivity to samples.

2.3.5. Water Uptake

Water absorption of samples was carried out in triplicate by immersion of samples ($80 \times 10 \times 4$ mm^3) in distilled water at room temperature following ISO 62:2008. Samples were extracted at different times and appropriately weighed using an analytical balance with an accuracy of ± 0.001 g, after removing the residual water with a dry cloth. Before the initial water immersion, samples were dried at 60 °C for 24 h to remove residual moisture. Water absorption percentage was calculated by using the following expression:

$$\text{Water uptake } (\%) = \frac{(W_t - W_0)}{W_0} \times 100 \tag{1}$$

where W_t is the dry weight of the sample after the corresponding time t, and W_0 is the initial weight of the sample before water immersion. The evolution of water uptake was followed in a total period of 12 weeks.

The diffusion coefficient (D) for all samples was calculated by the application of the first Fick's law using the following equation [54]:

$$D = \pi \left[\frac{mh}{4} \right]^2 \tag{2}$$

where m is a slope value, that can be calculated from the plot of W_t/W_s (dry weight after the corresponding time/saturation weight of the sample) versus $t^{1/2}$, and h stands for the initial thickness of the sample.

The previous equation for the calculation of D is only valid for a one-dimensional shape. To obtain the accurately corrected diffusion coefficient (D_c) for three-dimensional shapes, the Stefan approximation was applied, which assumes that the diffusion rates are the same for all directions [18]:

$$D_c = D \left[1 + \frac{h}{L} + \frac{h}{w} \right]^{-2} \tag{3}$$

where L and w are the length and width of each sample, respectively.

2.3.6. Color Properties

The influence of the FF content and size in the color of BioEP/FF composites were studied in a colorimeter model KONICA CM-3600d Colorflex-DIFF2 from Hunter Associates Laboratory (Virginia, EEUU). The CIELab color scale was used to measure the degree of L^* (lightness), a^* (color coordinate from red to green) and b^* (color coordinate from yellow to blue). The total color difference (ΔE) was calculated using the following equation:

$$\Delta E = \sqrt{(\Delta L^*)^2 + (\Delta a^*)^2 + (\Delta b^*)^2} \tag{4}$$

where ΔL^*, Δa^*, and Δb^* are the differences between the corresponding color parameter of the composites and the color parameter values of the reference material, i.e., BioEP matrix. Measurements were done in triplicate.

3. Results and Discussion

3.1. Morphology of FF Particles

Figure 2 shows the FESEM images of the flax flour powder, as well as the particle size distribution after each grinding process. Figure 2 includes representative images of each particle size at different magnifications while the particle size distribution plots were obtained by taking at least 50 measurements on different FESEM images corresponding to each particle size, namely fine (F) or coarse (C), using the software analysis included in the FESEM microscope. The following parameters were obtained (area, angle, and length), and the histogram plots included the length.

As can be seen in the FESEM images at lower magnifications (Figure 2a,d), coarse particles obtained by simple grinding (CFF) as well as fine flax flour particles with smaller dimensions (FFF), tend to form aggregates due to their high hydrophilicity. Quantitatively we can see from the size distribution made by measuring randomly chosen particles (Figure 2c,f), that CFF offers a particle size of 100–220 μm with an average particle size around 157 μm and remarkably higher particle content in the 140–160 μm range. On the other hand, FFF particle distribution shows that their size changes in the 40–140 μm range with smaller average particle size, of about 91 μm, and the most abundant content of particles is in the range of 80–100 μm. Therefore, it is evident that with the grinding of FF by ultra-centrifugation, finer particle sizes were obtained, which resulted in a better filler dispersion in the

matrix, as well as improved polymer-filler interactions, with a positive effect on the general properties of the developed composites.
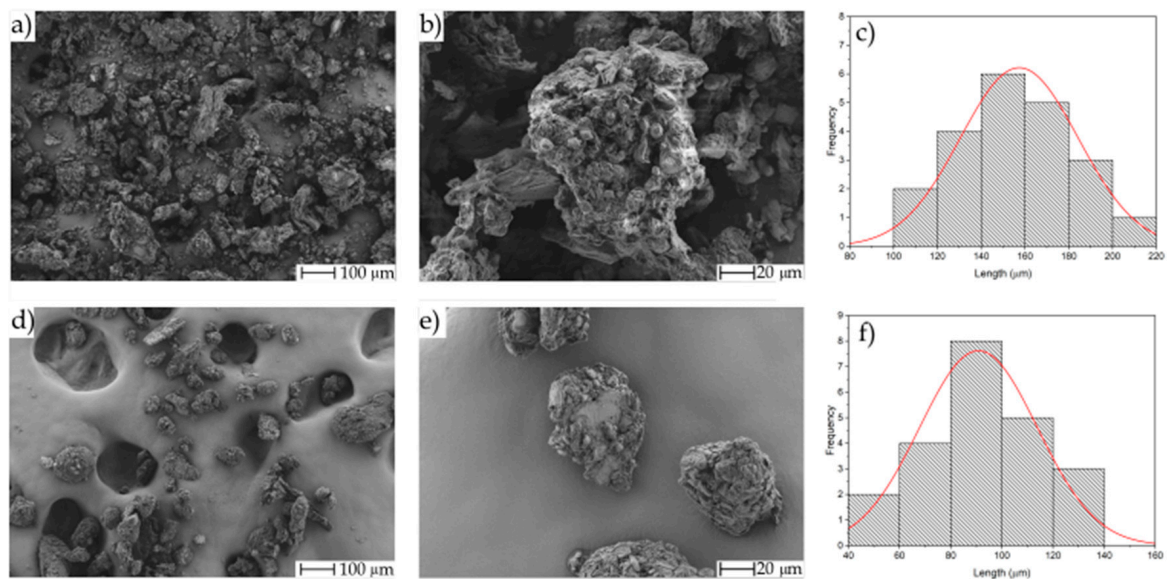

Figure 2. Field emission scanning electron microscope (FESEM) images corresponding to (**a**) CFF at 100× with a scale marker of 100 µm; (**b**) CFF at 500× with a scale marker of 20 µm; (**c**) particle size histogram of CFF; (**d**) FFF at 100× with a scale marker of 100 µm; (**e**) FFF at 500× with a scale marker of 20 µm; (**f**) particle size histogram of FFF.

The grinding process has a relevant effect on both particle aggregate and geometry. Despite this, these differences can be seen in Figure 2 since in general, both CFF and FFF particles had an irregular morphology with a rough surface and the presence of granular fractures (typical morphology of hard lignocellulosic particles after being subjected to crushing processes [54–56]). Figure 3 shows in a more detailed way the above-mentioned effects. Figure 3a shows the morphology of directly ground flax particles after the cold press process. One can see these particles show very irregular shapes. Moreover, it is possible to find particles with high size and very small particles. This is because no particle size separation has been carried out after this grinding process which led to coarse flax flour (CFF). In addition, aggregate formation is evident (in fact, the adhesive carbon tape cannot be seen).

Regarding fine flax flour (FFF), as shown in Figure 3b, it is evident that the shape is more likely spherical, the particle size range is narrower, and the aggregation phenomenon is less pronounced. The sieving process after ultra-centrifugation gives more homogeneity on the obtained morphologies and less aggregation.
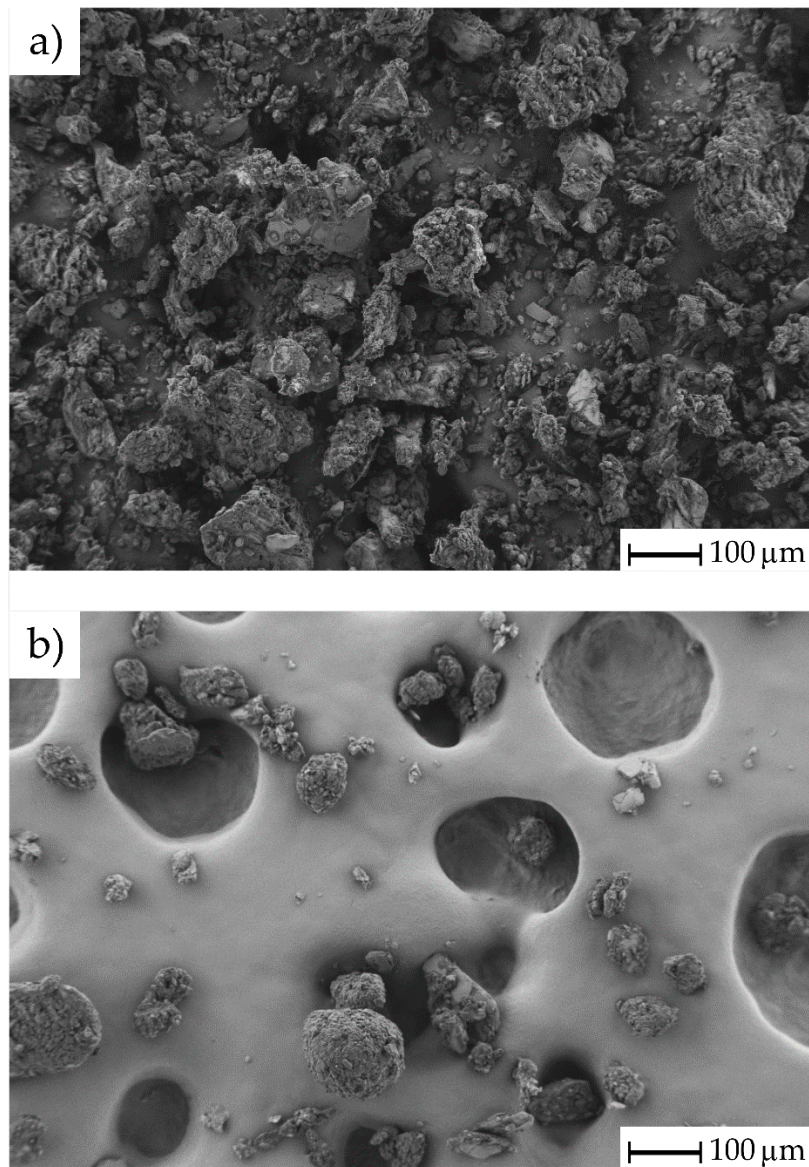
Figure 3. FESEM images corresponding to (**a**) CFF at 100× with a scale marker of 100 μm; (**b**) FFF at 100× with a scale marker of 100 μm.

3.2. Mechanical Properties

Table 1 shows the mechanical behavior of unfilled BioEP resin and BioEP/FF composites reinforced with different contents of CFF and FFF. Regarding the flexural properties, it can be seen that FF addition to the BioEP matrix results in a significant decrease in flexural strength compared to the unfilled BioEP resin. This decrease is much more pronounced as the FF content (both CFF and FFF) increases. As expected, the lowest flexural strength is obtained in composites reinforced with 40 wt% of CFF and FFF, obtaining a flexural strength of 22.5 and 22.9 MPa, respectively, which represents a decrease of 76.4% and 75.9% in comparison to the flexural strength of the unfilled BioEP resin (95.2 MPa). This decrease in flexural strength is due to the lack of adhesion between the lignocellulosic filler and the surrounding matrix, which causes stress concentration phenomena that promote breakage [20]. Another issue with a high influence on the mechanical properties of composites is the filler aspect ratio. High filler aspect ratios (above 6) result in a better stress transfer from the matrix to the filler/reinforcement, thus improving their mechanical properties. However, this stresses transfer is poorer in the case of low aspect ratio filler, such as the FF used, with an aspect ratio comprised between 1–2 [57]. If the two types

FF, i.e., coarse and fine FF (CFF and FFF, respectively) are compared, it can be seen that the flexural strength is always lower for all composites containing CFF. This is because the bigger particle size causes a larger weak interfacial area between the BioEP resin and the reinforcement, i.e., it decreases the adhesion between the hydrophobic matrix and the hydrophilic reinforcement which generates an increase in the stress concentration phenomena that negatively affect the mechanical properties of composites [58]. The biggest difference in flexural strength between composites with CFF and FFF is obtained for samples with 10 wt% of FF. For this composition, the flexural strength was 24.2% higher for FFF-reinforced composite compared to CFF-reinforced composite.

Table 1. Summary of the main mechanical properties of BioEP and BioEP/FF composites reinforced with different content of coarse (CFF) and fine (FFF) flaxseed flour particles obtained by flexural, impact, and hardness tests.

Code	Flexural Properties		Impact Energy $(kJ\ m^{-2})$	Hardness (Shore D)
	FS (MPa)	E_f (MPa)		
BioEP	95.2 ± 3.4	2985 ± 115	21.8 ± 3.4	83.2 ± 1.0
BioEP_10CFF	40.4 ± 1.3	2840 ± 242	2.7 ± 0.9	83.3 ± 0.6
BioEP_20CFF	31.5 ± 0.5	2878 ± 86	2.6 ± 0.6	82.3 ± 1.0
BioEP_30CFF	28.0 ± 2.0	2930 ± 93	2.4 ± 0.2	82.2 ± 1.0
BioEP_40CFF	22.5 ± 0.8	2290 ± 127	2.2 ± 0.3	81.0 ± 1.0
BioEP_10FFF	50.2 ± 1.4	3579 ± 53	3.6 ± 0.5	83.3 ± 1.0
BioEP_20FFF	38.7 ± 7.0	2975 ± 84	3.4 ± 0.1	83.7 ± 0.5
BioEP_30FFF	31.8 ± 1.5	2696 ± 20	2.7 ± 0.4	83.0 ± 1.1
BioEP_40FFF	22.9 ± 2.4	2108 ± 204	2.4 ± 0.2	81.6 ± 0.8

Regarding the flexural modulus, different trends can be observed for each of the fillers. The flexural modulus of CFF-reinforced composites is hardly affected by 10, 20, and 30 wt% filler and the modulus values are similar to those obtained for BioEP resin (2840–2985 MPa). However, the flexural modulus of the composite reinforced with 40 wt% CFF decreases significantly to 2290 MPa, representing a decrease of 23.3% compared to the unfilled BioEP resin. This is directly related to an embrittlement process which is much more evident at higher filler loadings. It is important to bear in mind that the flexural modulus is directly related to the supported stress and inversely related to the flexural deformation. BioEP is intrinsically brittle, therefore, the change in the flexural deflection before fracture is very low. This is even reduced in BioEP/FF composites, but the most important parameter is a clear decrease of the flexural strength from 95.2 MPa down to 22.9 MPa. For this reason, at 40 wt% CFF, the modulus decreases in a remarkable way since the flexural stress is remarkably reduced while the elongation is almost identical to neat BioEP, which is an intrinsically brittle material.

In the case of FFF-reinforced composites, the addition of 10 wt% FFF to the BioEP matrix significantly increases the flexural modulus from 2985 MPa (unreinforced BioEP) resin up to 3579 MPa, which is a % increase of nearly 20%. This increase in the flexural modulus compared to the 10 wt% CFF reinforced composite may be due to the better dispersion of fine particles into the matrix and improved polymer-particle interaction due to its smaller size, which results in comparatively higher flexural strength values, and consequently higher modulus and stiffness. It should be noted that the sample reinforced with 10 wt% FFF has similar and even higher flexural mechanical properties than those obtained in commercial WPCs currently used in furniture applications [59,60]. For higher FFF contents, it is observed that the flexural modulus decreases as the reinforcement content increases, obtaining the lowest modulus for the sample reinforced with 40 wt% FFF, 2108 MPa, which shows the same behavior above-mentioned.

Regarding the impact energy (Charpy test), it can be seen in Table 1, that the incorporation of both CFF and FFF in the BioEP resin results in a remarkable decrease in impact-absorbed energy from 21.8 kJ m^{-2} corresponding to the unfilled BioEP resin to values around 3 kJ m^{-2} for FF reinforced composites. This behavior is typical of polymeric composites filled with lignocellulosic particles due

to the lack of (or very poor) interfacial adhesion between the reinforcement and the matrix, which gives rise to stress concentration points, promoting the formation of microcracks at the interface when impact conditions are applied that easily induce crack propagation, thus decreasing their impact resistance [61,62]. Impact energy absorption is also influenced by the filler content in the matrix. As can be seen, the impact energy absorption becomes lower as the reinforcement content increases, obtaining the lowest impact-absorbed energy for composites reinforced with 40 wt% CFF and FFF, with an impact energy of 2.2 and 2.4 kJ m^{-2} respectively, which represents a decrease of nearly 90% in both cases with respect to the BioEP resin. This decrease in impact energy with the higher filler content is due to the greater lack of interaction between the filler and the matrix, which results in a higher void content, thus increasing the stress concentration phenomena. Particle size is another factor affecting the impact of energy absorption. When comparing the composites, the energy absorption values for the different percentages of reinforcement are slightly lower in the case of CFF-reinforced composites. This is because the coarse particles have less dispersion in the matrix as well as a larger surface area that leaves a greater amount of surface-exposed between the filler and the matrix, negatively affecting the mechanical properties [63]. It is worthy to note that the better results regarding mechanical properties, obtained with FFF were expected as the morphology of FFF is rounded (almost spherical in most cases) while CFF show very irregular shapes with angular geometries that contribute to micro crack formation and subsequent growth.

Regarding the Shore D hardness, it can be seen in Table 1 that the incorporation of the FF filler into the BioEP matrix hardly affects hardness. Only a slight decrease is seen in samples reinforced with 40 wt% CFF and FFF, in which a hardness of 81.0 and 81.6 Shore D, respectively, was obtained, which means a decrease of 2.6% and 1.9%, respectively, in comparison to the BioEP resin hardness (83.2 Shore D). The slight decrease in hardness in composites reinforced with a high amount of FF may be due to the lower lignocellulosic reinforcement hardness compared to the thermosetting matrix used [58]. By considering these mechanical properties, it seems that composites with 10 wt% FFF offer the best-balanced properties. Despite this, other compositions must not be discarded as they offer a higher biobased content and wood-like surface finish. Obviously, these high wt% FF composites would not be suitable for technical applications since there brittle and with low tensile strength, but they can find interesting applications in the decorative sector and leather goods (buckles, buttons, among others).

3.3. Thermal Properties

The thermal stability at high temperatures of FF, BioEP resin, and different BioEP/FF composites was obtained by thermogravimetric analysis (TGA). The temperature effect on the mass of each sample is shown in Table 2, while Figure 4 shows the corresponding TGA and DTG curves for FF, BioEP resin and BioEP/FF with varying CFF and FFF content from 10 to 40 wt%.

Table 2. Thermal parameters of BioEP and BioEP/FF composites reinforced with different contents of coarse (CFF) and fine (FFF) flaxseed flour, obtained by thermogravimetry (TGA).

Code	T_0 [1] (°C)	T_{max} (°C)	wt% Residual Mass
BioEP	306.0 ± 2.1	327.5 ± 1.7	8.5 ± 0.3
BioEP_10CFF	292.7 ± 2.8	322.2 ± 2.5	12.9 ± 0.4
BioEP_20CFF	273.7 ± 1.9	322.2 ± 1.9	13.5 ± 0.5
BioEP_30CFF	268.0 ± 3.1	322.0 ± 2.5	15.0 ± 0.6
BioEP_40CFF	249.2 ± 2.0	323.2 ± 1.4	18.7 ± 0.6
BioEP_10FFF	279.2 ± 1.0	322.2 ± 1.8	10.1 ± 0.5
BioEP_20FFF	270.1 ± 2.4	323.0 ± 3.2	12.7 ± 0.4
BioEP_30FFF	264.0 ± 1.6	321.1 ± 1.8	15.7 ± 0.3
BioEP_40FFF	244.2 ± 2.2	319.0 ± 2.1	20.3 ± 0.4

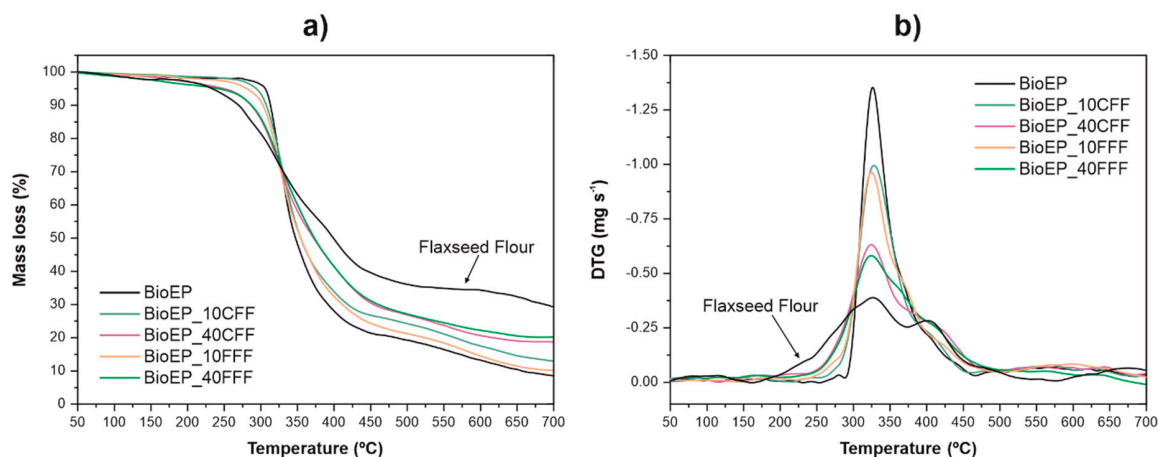[1]T_0, calculated at 5% mass loss.

Figure 4. Thermal degradation of BioEP, FF, and BioEP/FF composites reinforced with a different content of coarse (CFF) and fine (FFF) flaxseed flour (**a**) thermogravimetry (TG) weight loss and (**b**) differential thermogravimetry (DTG) first derivative curves.

As shown in Figure 4a, the FF showed four typical degradation stages of lignocellulosic materials. In the first stage, produced at 50–150 °C, the moisture contained in the material evaporated, which was reflected by a mass loss of around 2.3 wt% [64]. In the second stage thermal depolymerization of hemicelluloses took place in the temperature range from 150 to 375 °C with a weight loss of about 41.4% [65]. In the third stage, which was located at 375–450 °C, cellulose degradation occurred, this stage being observed by a weight loss of 18.9% [61]. Finally, the lignin degradation was detected, which begins at around 250 °C, but due to its complex structure, it degraded more slowly, producing a progressive weight loss up to 500 °C. Its decomposition being overlapped with that of other compounds [14]. As shown in the TGA graph, the residual mass of FF was high, which can be due to its high mineral content [66]. On the other hand, as can be seen in Table 2, the thermal degradation of the BioEP resin occurred in a single step, starting its degradation (T_0) around 306 °C and with a maximum degradation temperature (T_{max}) of 327.5 °C. Regarding BioEP/FF composites degradation, it can be seen that the FF filler addition to the matrix results in a slight decrease of the composites' thermal stability, which is reflected by a T_0 decrease.

This is due to the low thermal stability of the lignocellulosic reinforcement, whose degradation onset temperature begins around 234 °C, which affects the overall thermal stability of composites negatively. Besides, the increased filler content in composites results in a reduced weight fraction of the BioEP resin, causing a more significant decrease in T_0 as the filler content increases [20]. Comparing the two types of composites obtained according to the filler size, it can be seen that the thermal stability was slightly lower, i.e., lower T_0, for composites with different FFF contents. This lower thermal stability was more evident for composites with 10 wt% FFF, where a decrease in T_0 of 27 °C compared to the T_0 of the BioEP resin can be observed, while this decrease is only 13 °C for the same composite containing 10 wt% CFF. By observing the DTG curves (Figure 4b) it can be seen that the thermal degradation of BioEP/FF composites takes place in two stages. These stages were more evident in the reinforced samples with high filler contents (40 wt%). In the first stage, BioEP resin was thermally degraded along with the low molecular weight components of FF such as hemicelluloses, while in the second stage the thermal degradation of cellulose and lignin occurred. For this reason, this stage was more evident in composites with high filler content. Regarding the maximum degradation temperature (T_{max}), obtained from the peak of the first degradation stage of the DTG curves, it can be seen that the incorporation of the reinforcement into the BioEP matrix slightly decreases this temperature (it almost remains constant). In this case, the T_{max} of composites did not vary significantly with the particle size or content, obtaining a T_{max} of around 322 °C for all developed composites, except for the composite reinforced with 40 wt% of FFF, which has a T_{max} slightly lower of about 319 °C. Therefore, after thermogravimetric analysis, the results suggest that as the lignocellulosic reinforcement

content increases, the thermal stability of the composites decreases, while the residual mass at high temperatures (700 °C) increases. Nevertheless, the overall thermal stability of these composites is not compromised by incorporating FF in both coarse and fine particle size.

3.4. Morphological Properties

The particle dispersion and its interaction with the matrix are two of the main aspects that influence the composite's mechanical properties. To study these phenomena, a morphological study was carried out using FESEM on impact fractured surfaces of BioEP resin and BioEP/FF composites filled with 10 wt% and 40 wt% CFF and FFF. Figure 5a shows the BioEP resin fracture surface, which is characterized by a smooth surface with the presence of cleavage planes characteristic of a brittle fracture.
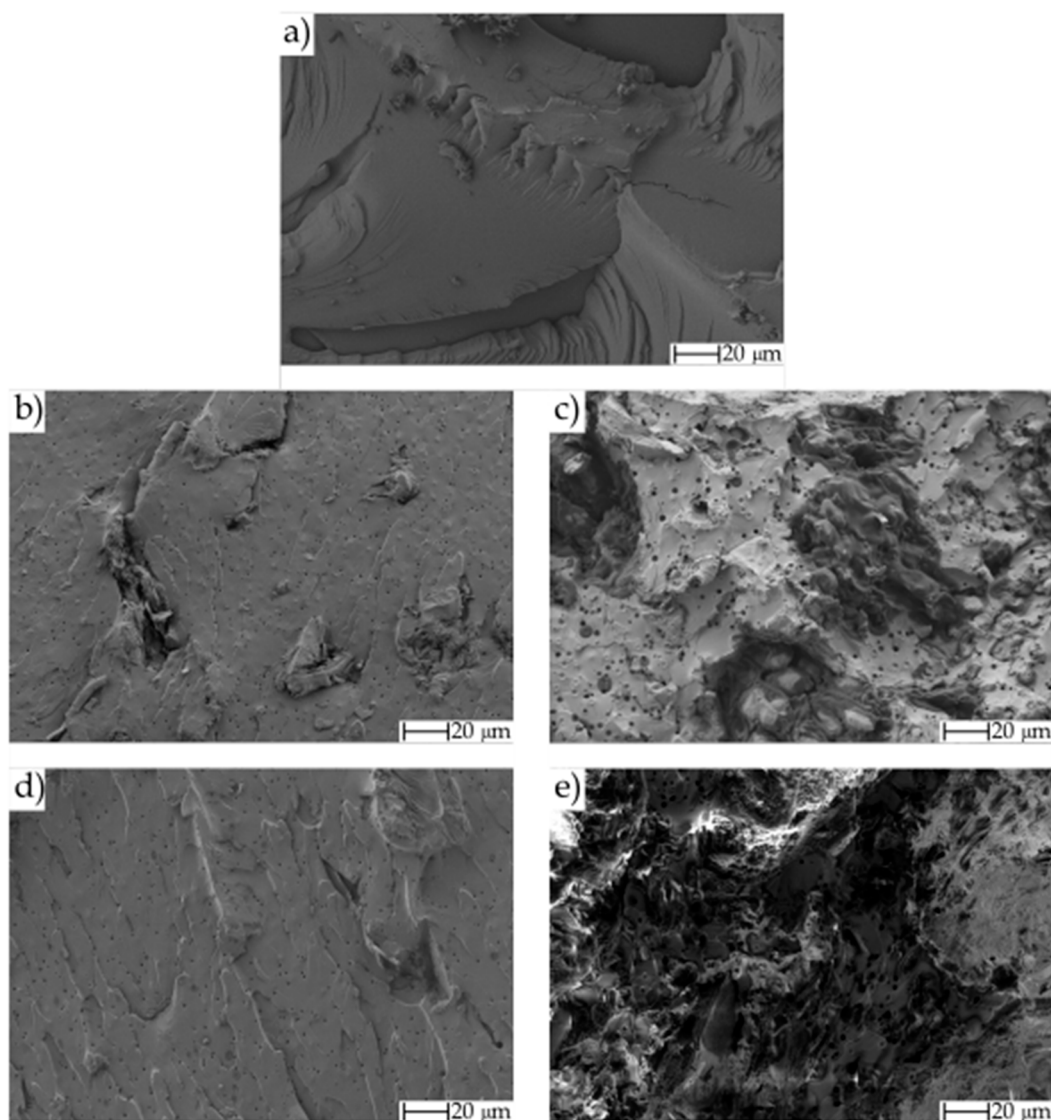

Figure 5. FESEM images at 500× of impact-fracture surface of: (**a**) BioEP; (**b**) BioEP_10CFF; (**c**) BioEP_40CFF; (**d**) BioEP_10FFF and (**e**) BioEP_40FFF.

After the addition of 10 wt% of both CFF and FFF filler (Figure 5b,d), it can be seen that the fracture surface acquires a noticeable roughness, and small holes appear randomly located on the surface, which corresponds to the particles pulled out after the impact test. These voids/holes are representative of poor adhesion between the polymeric matrix and the lignocellulosic filler, which

results, as above-mentioned, in low stresses transfer from the matrix to the filler, thus negatively affecting the overall mechanical properties of the obtained composites. Comparing the two types of composites reinforced with 10 wt% FF, it can be seen that fine particles (FFF) reinforced composites, a better particle dispersion in the matrix is achieved due to the smaller particle size, which is reflected in the absence of aggregates in the fracture surface. Such aggregates are observed on the fracture surface of the coarse particles (CFF) reinforced composites, as the larger particle size promotes their aggregation. The higher lack of adhesion between these aggregates and the matrix due to the increase of the exposed surface area intensifies the stress concentration phenomena that negatively affects the mechanical properties, as it has been evidenced by a lower impact energy absorption and lower flexural strength than the composite reinforced with 10 wt% FFF. Higher filler contents (Figure 5c,e) lead to an increase in the fracture surface roughness with the presence of particles embedded in the matrix. An increase in the size of the voids/holes was also observed, possibly because the higher filler content promoted aggregate formation. This increase in the void size results in reduced interfacial adhesion between the reinforcement and the matrix for composites reinforced with high FF contents, which is reflected in poor mechanical properties. Comparing both composites reinforced with 40 wt% of FF, the presence of large aggregates in the CFF reinforced sample can be seen more clearly, while in the FFF reinforced sample, the dispersion of particles was more homogeneous. Therefore, the increase of the filler content in the matrix results in a significant decrease in ductile and resistant mechanical properties, as shown by the evolution of impact energy absorption and flexural strength, due to a reduction in interfacial adhesion between filler and matrix by a decrease in the resin's ability to fully embed the particles. This also occurs with coarse particles (CFF), which have a higher surface area, exposing more surface area to weak bonding with the matrix, resulting in lower flexural strength and higher water absorption capacity.

3.5. Thermo-Mechanical Properties

Figure 6 shows the evolution of the storage modulus (G') and the dynamic damping factor ($tan\ \delta$) as a function of the temperature of BioEP resin and BioEP composites reinforced with 10 wt% and 40 wt% of CFF and FFF. On the other hand, Table 3 shows the storage modulus at 40 °C and 110 °C, as well as the glass transition temperature (T_g), obtained from the peak maximum of the $tan\ \delta$ curve for all considered composites.
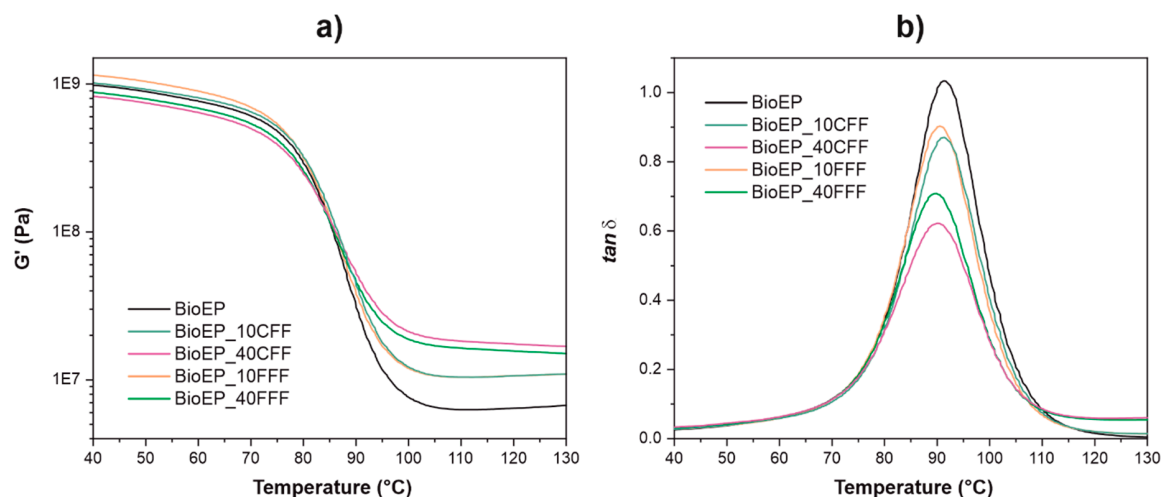

Figure 6. A comparative plot of the dynamic mechanical thermal analysis (DMTA) behavior of BioEP and BioEP/FF composites reinforced with CFF (10 and 40 wt%) and FFF (10 and 40 wt%): (**a**) storage modulus (G'), and (**b**) dynamic damping factor ($tan\ \delta$).

Table 3. Values of dynamic mechanical, thermal analysis (DMTA), and thermomechanical analysis (TMA) of BioEP and BioEP composites reinforced with different CFF and FFF content.

Code	DMTA			TMA	
	G′ at 40 °C (MPa)	*G′* at 110 °C (MPa)	T_g (°C)	*CLTE* below T_g (μm m^{-1} K^{-1})	*CLTE* above T_g (μm m^{-1} K^{-1})
BioEP	981 ± 25	6.3 ± 0.3	91.8 ± 2.1	0.356 ± 0.008	0.565 ± 0.005
BioEP_10CFF	1015 ±36	10.4 ± 0.2	90.8 ± 2.7	0.395 ± 0.015	0.938 ± 0.005
BioEP_20CFF	1041 ± 58	12.5 ± 0.3	90.7 ± 1.7	0.385 ± 0.002	0.621 ± 0.005
BioEP_30CFF	1091 ± 49	18.4 ± 0.9	89.8 ± 2.5	0.570 ± 0.006	0.813 ± 0.005
BioEP_40CFF	826 ± 30	18.5 ± 0.8	90.2 ± 2.5	0.404 ± 0.010	0.727 ± 0.007
BioEP_10FFF	1147 ± 13	10.4 ± 0.2	89.8 ± 2.1	0.529 ± 0.013	0.824 ± 0.003
BioEP_20FFF	1064 ± 52	11.5 ± 0.3	89.1 ± 1.8	0.380 ± 0.009	0.687 ± 0.006
BioEP_30FFF	935 ± 40	14.1 ± 0.4	89.2 ± 1.6	0.436 ± 0.007	0.635 ± 0.002
BioEP_40FFF	878 ± 24	16.3 ± 0.4	89.9 ± 2.2	0.554 ± 0.002	0.770 ± 0.001

The storage modulus (*G′*) (Figure 6a) shows different behavior depending on the filler content. As shown in Table 3, the addition of a lignocellulosic filler into the BioEP resin hardly affects the storage modulus at low temperatures (40 °C), resulting in very similar G′ values to the unfilled BioEP resin. However, at high temperatures (110 °C), it can be seen more clearly how the filler content leads to an increase in *G′*. As observed in Figure 6a, *G′* increases as the filler content increases, resulting in more rigid materials as the FF content increases. This is because the particles give rise to a high degree of mechanical restriction since they act as interlock points that reduce the mobility of the polymeric 3D-thermosetting net and their deformation ability. This phenomenon is much more pronounced at high temperatures when the chain motion or vibration is greater [22,61]. Comparing the composites according to the type of reinforcement, it can be seen that the reinforced composites with coarse particles (CFF) have a higher modulus at high temperatures, thus showing their higher capacity to maintain the mechanical load with recoverable viscoelastic deformation at high temperatures compared to the FFF-reinforced composites [56]. Figure 6b shows the dynamic damping factor (*tan δ*) evolution regarding temperature. As can be seen, the BioEP resin curve has the highest value of *tan δ*; however, this value decreases as the FF content in the matrix increases.

This decrease is due to the attenuation that the addition of the filler stiff domains causes in the resin since filler particles act as a steric hindrance [56]. As shown in Table 3, the T_g of the BioEP resin, obtained from the peak maximum of the dynamic damping factor, is around 92 °C. After the addition of the lignocellulosic filler, the T_g remains almost constant, with slight changes due to the restriction that the rigid particles randomly dispersed in the epoxy matrix cause [51]. Comparing both composites, it can be seen that the T_g decrease is slightly higher for FFF-reinforced composites, with a T_g of around 89 °C for all of them, on the other hand, it can be seen that T_g obtained for CFF-reinforced composites is about 90 °C. This slight difference in T_g between the two composites may be because the smaller size of the particles and the greater dispersion of them in the matrix results in greater interaction between the filler and the matrix and, therefore, the mobility of the polymer chains in these regions are more restricted [67]. Despite this hypothesis, the changes in T_g are so slight that it is not possible to hypothesize a remarkable effect of the filler on T_g. In addition, it is worthy to note that FF has been obtained after cold-pressing flaxseed and some residual oil could be present in the flour, thus explaining this slight decrease in T_g [68].

To analyze the dimensional stability of the obtained composites, the coefficient of linear thermal expansion (*CLTE*) was determined by thermomechanical analysis (TMA). Table 3 shows the *CLTE* of BioEP resin and FF-reinforced BioEP composites obtained from the slope of the thermal expansion curves in the rubbery (above T_g) and glassy (below T_g) regions. As shown in Table 3, the BioEP resin shows a low *CLTE*, both below and above the T_g, characteristic of thermosetting resins, which usually exhibit excellent dimensional stability [69]. As can be seen, the *CLTE* is lower for all the samples obtained at temperatures below T_g. This is due to the lower mobility of the polymeric chains in

the glassy state, which results in low values of linear expansion [70]. Concerning *CLTE* below T_g, it was observed that the addition of FF filler to BioEP resin increased its value, which evidenced lower dimensional stability of composites with respect to BioEP resin; nevertheless, the dimensional stability of these composites was not compromised since the *CLTE* values obtained for all composites were still very low. In Table 3, it can be seen how the *CLTE* values below T_g in the developed composites did not show any clear trend regarding the filler content. This was also observed for *CLTE* above T_g, where there was an increase in this value after the addition of FF filler into the BioEP resin, but there was no trend with respect to the filler content used in the matrix. In this case, it can be seen how the lowest dimensional stability of the developed composites was obtained for composites filled with 10 wt% for both types of filler size, CFF and FFF, with *CLTE* values of 0.938 and 0.824 μm m^{-1} K^{-1} respectively. Despite this slight increase, the dimensional stability of the developed composites was very high compared to conventional WPCs with *CLTE* values higher than 50 μm m^{-1} K^{-1} [71–73].

3.6. Water Uptake Properties

Figure 7 shows the evolution of the water absorption over time for BioEP resin and BioEP/FF composites filled with 10 wt% and 40 wt% of CFF and FFF. The water diffusion in the wood plastic composites is based on three different mechanisms, the first one involves the water molecules diffusion inside the micro-voids of the polymeric chains, the second mechanism is based on the water absorption by capillarity inside the voids and defects present at the matrix-filler interface, finally, the third mechanism involves the transport through the micro cracks that appear from the swelling of the fillers, namely, the swelling of the reinforcement produced by the contact with the water gives rise to the appearance of microcracks in the fragile thermosetting resin, which facilitates its penetration in the interface between the filler and the matrix [74]. As can be seen in Figure 7, the addition of FF into the BioEP resin significantly increased its water absorption capacity, which rose as the reinforcement content in the matrix increased. This could be due to two possible reasons, one of them is to the hydrophilic nature of the lignocellulosic filler, since cellulose and hemicellulose contain hydroxyl (-OH) groups in their structure that can easily interact with water molecules through hydrogen bonding, thus allowing a path for water entering [61,75]. The other reason is the presence of small voids, pores and microcracks in the internal structure due to the lack of interfacial interaction between the filler and matrix and to the filler swelling. that facilitates the water accumulation in the composite by capillarity [24,76]. By observing the water absorption curves of BioEP/FF composites, two stages can be clearly differentiated. We can see an initial stage with rapid water absorption, followed by a second stage where the curve stabilized into an asymptotic value, thus indicating saturation. Therefore, the water absorption of BioEP/FF composites followed Fickian's diffusion behavior. However, at low immersion times, Figure 7a, it can be seen how the weight gain in the curves of the composites stops being gradual and a rapid increase in weight appears between 10 and 12 h of immersion in all of them. This can be due to the appearance of deformations or damage to the matrix for that immersion time, such as the appearance of microcracks due to the swelling of the filler or the fiber/matrix debonding [77]. As shown in Table 4, the water saturation of composites increases as the filler content does. In this case, it can be seen how the water saturation of composites reinforced with 10 wt% of FF (both CFF and FFF) reaches values of 4.8 wt%. Obviously, composites with 40 wt% of FF water saturation are located at about 12.5 wt%, which means an increase in water absorption compared to neat BioEP resin of 114.3% and 458% respectively. A comparison of the two types of composites obtained shows that CFF-reinforced composites have a slightly higher water absorption compared to their FFF counterparts. This may be due to the larger particle size of the CFF filler, which results in less interaction with the matrix, producing a higher number of voids within the structure of composites. These voids allow the accumulation of water at the interface between the particle and the matrix thus increasing the absorption capacity of the composites [78]. In addition, the increased contact between FF particles as their size and content in the matrix increases contributes to water absorption by capillarity due to the creation of a percolating path through the filler network [79]. It should be noted that the water

absorption of FF waste is lower than that obtained from other agroforestry waste that has been used in similar amounts as reinforcements in thermosetting polymeric matrices, such as peanut shells [63] or palm kernel shell [80]. As can be seen in Figure 7, there are some slight differences between the sort-term behavior (first 24 h, Figure 7a) and the long-term behavior (90 days immersion, Figure 7b). Despite this visual difference, it is worthy to note the scale. For the short-term graph, some specimens do not follow the expected behavior (e.g., BioEP/CFF 10 wt%), but the changes in the water absorption are very low, of about 0.2–0.3 wt%, which could be even included in the measurement error. In addition, this initial stage (24 h), is very sensitive to the surface, i.e., the presence of particles not fully embedded and directly exposed to water, which could cause these slight changes. The stationary water absorption after 90 days, represents the actual water uptake behavior as all these initial phenomena disappear, and this agrees with the expected behavior in terms of particle size and loading.
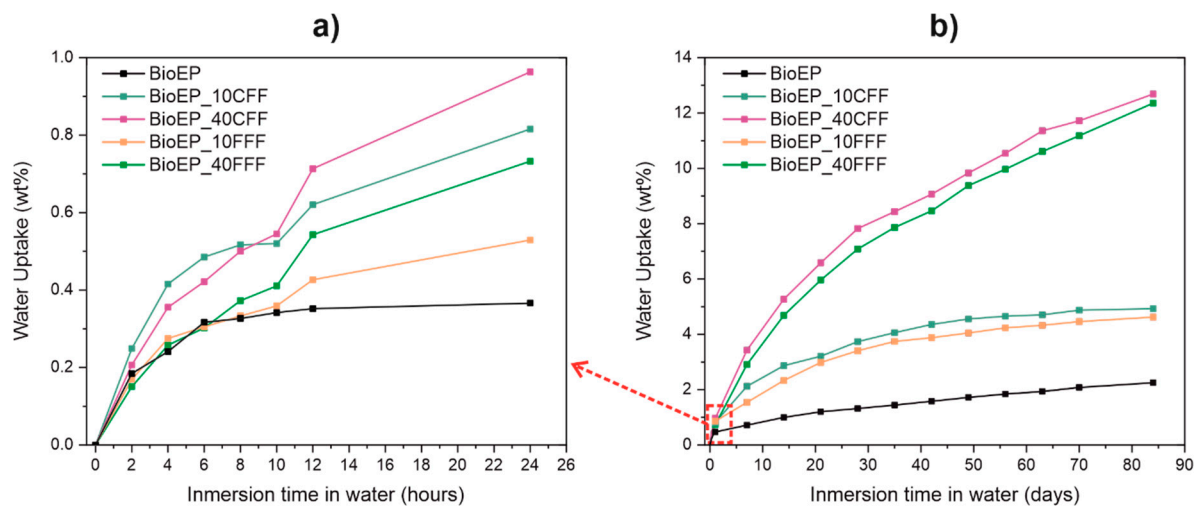

Figure 7. Evolution of water absorption over time of BioEP resin and BioEP composites filled with CFF (10 and 40 wt%) and FFF (10 and 40 wt%): (**a**) water absorption during the first 24 h; (**b**) water absorption during a period of 12 weeks.

Table 4. Values of water saturation (W_s), diffusion coefficient (D) and the corrected diffusion coefficient (D_c) for BioEP resin and BioEP composites reinforced with different CFF and FFF content.

Code	W_s (wt%)	$D \times 10^{-9}$ (cm^2 s^{-1})	$D_c \times 10^{-9}$ (cm^2 s^{-1})
BioEP	2.2 ± 0.0	0.72 ± 0.90	0.36 ± 0.42
BioEP_10CFF	4.9 ± 0.1	1.51 ± 0.40	4.99 ± 2.03
BioEP_20CFF	7.5 ± 0.1	2.07 ± 0.06	6.84 ± 2.9
BioEP_30CFF	8.4 ± 0.2	3.35 ± 0.10	11.1 ± 2.5
BioEP_40CFF	12.7 ± 0.1	4.27 ± 0.05	14.2 ± 0.9
BioEP_10FFF	4.6 ± 0.1	1.38 ± 0.01	4.56 ± 0.2
BioEP_20FFF	6.5 ± 0.1	2.23 ± 0.05	7.37 ± 0.6
BioEP_30FFF	7.7 ± 0.1	2.39 ± 0.04	7.9 ± 0.8
BioEP_40FFF	12.4 ± 0.1	3.39 ± 0.05	11.2 ± 0.9

Table 4 shows the values of the saturation by weight (W_s), as well as the diffusion coefficient (D) and the corrected diffusion coefficient (D_c) of BioEP resin and the obtained BioEP/FF composites. The diffusion coefficient is one of the most important parameters of the Fick's model, which is related to the initial diffusion of water molecules into the matrix surface by entering through external micro-voids towards the internal structure of the composites [81]. As can be seen, the BioEP resin is characterized by a W_s of 2.2 wt%, a D of 0.72×10^{-9} cm^2 s^{-1}, and a D_c of 0.36×10^{-9} cm^2 s^{-1}. After the incorporation of the highly hydrophilic lignocellulosic residue, it is observed, as expected, that D and D_c increase as the CFF and FFF content does, following the behavior shown by other composites reinforced with natural

fillers [18,82,83]. Therefore, it can be concluded that the increase in the amount of lignocellulosic filler increases the ability of water molecules to enter through the composite. Comparing both composites (with CFF and FFF), it can be seen how CFF-filled materials tend to have a higher diffusion coefficient than FFF-filled composites, mainly due to the larger particle size and the more significant presence of voids in the internal structure of the composite due to the lack of matrix-filler interaction [84].

3.7. Color Properties

Figure 8 shows the resulting visual aspect of BioEP resin and BioEP/FF composites filled with coarse particles-CFF (Figure 8a) and fine particles-FFF (Figure 8b) after the curing/post-curing cycle.
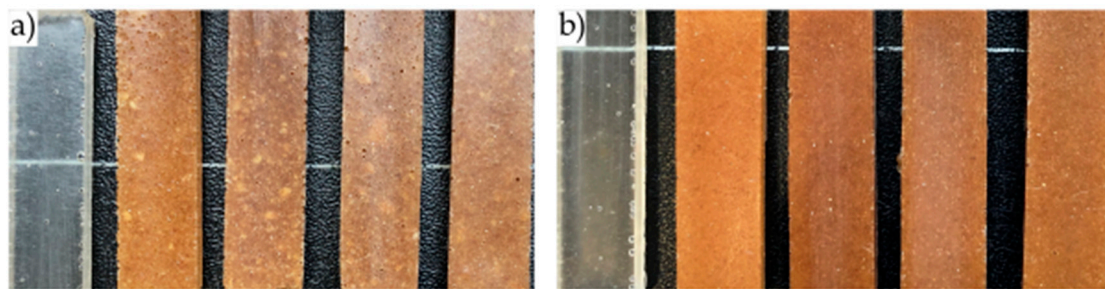
Figure 8. Visual aspect of BioEP and BioEP composites reinforced with different FF content; (**a**) (left to right) BioEP resin and BioEP composites reinforced with 10, 20, 30 and 40 wt% of CFF; (**b**) (left to right) BioEP resin and BioEP composites reinforced with 10, 20, 30 and 40 wt% of FFF.

Table 5 gathers the color parameters for the BioEP resin and BioEP/FF composites. As can be seen in Figure 8, BioEP/FF composites obtained by casting show dimensional uniformity as well as a uniform and defect-free surface appearance. This situation is even more evident in composites with FFF. As can be seen, the unfilled BioEP resin sample has some degree of transparency, which is reflected by the low $a*$ and $b*$ values. After the addition of the FF filler, composites become brown due to the natural color of the lignocellulosic filler (see Figure 1), which produces an increase in the values in the $a*$ and $b*$ coordinates (Table 5). As it can be seen in Figure 8, and quantitatively analyzed by the CIElab coordinates, the color of composites filled with FF is very similar in all of them except that with 10 wt% of FFF, which presents a lighter brown color, obtaining a lower ΔE with respect to the BioEP than the rest of the composites. Comparing both types of composites according to the filler size (CFF or FFF), it can be seen how the surface appearance of FFF-filled composites is much more homogeneous than CFF-filled composites. In the case of CFF-reinforced composites, random whitish spots are present on the surface, which may be due to the formation of large filler aggregates, which negatively affect both aesthetics and mechanical properties. The brown wood color acquired by the samples after the filler incorporation, and the excellent surface appearance acquired mainly in the samples reinforced with FFF can be attractive from the aesthetic point of view for applications in sectors such as furniture, construction, or automotive [85,86].

Table 5. Color parameters from the CIELab space of BioEP resin and BioEP composites reinforced with different CFF and FFF content.

Code	L*	a*	b*	ΔE
BioEP	39.50	−0.48	1.60	-
BioEP_10CFF	39.51	8.97	19.02	19.82
BioEP_20CFF	40.77	9.51	19.36	20.42
BioEP_30CFF	40.93	9.59	19.54	20.62
BioEP_40CFF	41.48	9.68	19.83	20.97
BioEP_10FFF	35.82	9.61	15.80	17.80
BioEP_20FFF	36.27	9.52	16.83	18.50
BioEP_30FFF	37.77	9.44	17.11	18.49
BioEP_40FFF	39.55	9.63	18.42	19.62

4. Conclusions

The main objective of the present work was to evaluate the influence of FF particle size, i.e., coarse (CFF) and fine (FFF), and the filler content (10, 20, 30 and 40 wt%) on the mechanical, thermal, water uptake and morphological properties of composites of a partially biobased epoxy (BioEP) resin processed by casting. The addition of this lignocellulosic filler into the BioEP matrix resulted in a decrease in flexural strength and impact absorption energy with increasing filler content. This is because of the lack of (or very poor) polymer matrix-particle filler interactions. However, this decrease is lower for composites with finer particles, due to their better dispersion and better interaction with the matrix. In this work, it has been observed that the composite filled with 10 wt% of FFF presents a flexural strength and impact energy absorption 24.2% and 33.3% higher than its counterpart with CFF. Particle size has also a high influence on water absorption. It has been observed that composites with fine particles (FFF) filler offer less water absorption due to the presence of fewer voids in their structure as a result of better dispersion and fewer aggregates. In the case of CFF-filled composites, the larger size increases the lack of adhesion with the matrix generating voids and aggregates that allow the water entering, thus leading to a higher water absorption and diffusion coefficient.

Therefore, the present work has revealed that the finer filler particle size results in better mechanical and water absorption properties in these natural fiber reinforced plastics (NFRPs). Besides, a partially biobased, high environmentally friendly material can be obtained. On one hand, the partial biobased epoxy content (31 wt%) can be increased up to almost 70 wt% renewable origin in composites with 40 wt% FF (both CFF or FFF). In addition, this work has revealed an alternative to upgrading wastes from the flaxseed industry. The developed BioEP/FF composites offer an attractive wood-like aesthetic appearance, and therefore, they can be used in sectors such as decoration, furniture, or the automotive industry.

Once the particle size and the amount of FF have been optimized to obtain more balanced mechanical, thermal and water absorption properties in the BioEP/FF composite, further studies will focus on the use of highly reactive coupling agents, i.e., silanes such as (3-glycidyloxypropyl) trimethoxy silane and (3-aminopropyl) trimethoxy silane, to provide increased interaction between the epoxy matrix and the embedded FF particles. All these steps, including an industrial scalation and cost study will assess the viability of these materials to contribute to the circular economy in the flax industry.

Author Contributions: Conceptualization, R.B. and T.B.; Data curation, D.L., D.G.-G. and T.B.; Formal analysis, D.L. and L.Q.-C.; Investigation, D.L. and S.R.-L.; Methodology, D.L., D.G.-G. and L.Q.-C.; Project administration, R.B. and T.B.; Supervision, D.G.-G. and R.B.; Validation, D.G.-G., R.B. and T.B.; Writing–original draft, D.L. and S.R.-L.; Writing–review & editing, D.G.-G. and R.B. All authors have read and agreed to the published version of the manuscript.

Conflicts of Interest: The authors declare no conflict of interest.

References

1. Antonio, C.; Newson, W.; Olsson, R.; Hedenquist, M.; Johansson, E. Advances in the use of protein-based materials: Towards sustainable naturally sourced absorbent materials. *ACS Sustain. Chem. Eng.* **2019**, *7*. [CrossRef]

2. Babu, R.P.; O'connor, K.; Seeram, R. Current progress on bio-based polymers and their future trends. *Prog. Biomater.* **2013**, *2*, 8. [CrossRef]

3. Kim, J.-Y.; Lee, H.W.; Lee, S.M.; Jae, J.; Park, Y.-K. Overview of the recent advances in lignocellulose liquefaction for producing biofuels, bio-based materials and chemicals. *Bioresour. Technol.* **2019**, *279*, 373–384. [CrossRef]

4. Boronat, T.; Fombuena, V.; Garcia-Sanoguera, D.; Sanchez-Nacher, L.; Balart, R. Development of a biocomposite based on green polyethylene biopolymer and eggshell. *Mater. Des.* **2015**, *68*, 177–185. [CrossRef]

5. Naghmouchi, I.; Mutjé, P.; Boufi, S. Olive stones flour as reinforcement in polypropylene composites: A step forward in the valorization of the solid waste from the olive oil industry. *Ind. Crops Prod.* **2015**, *72*, 183–191. [CrossRef]

6. Zaaba, N.F.; Ismail, H. Thermoplastic/Natural Filler Composites: A Short Review. *J. Phys. Sci.* **2019**, *30*, 81–99. [CrossRef]

7. Garcia-Garcia, D.; Carbonell-Verdu, A.; Jordá-Vilaplana, A.; Balart, R.; Garcia-Sanoguera, D. Development and characterization of green composites from bio-based polyethylene and peanut shell. *J. Appl. Polym. Sci.* **2016**, *133*. [CrossRef]

8. Torres-Giner, S.; Montanes, N.; Fenollar, O.; García-Sanoguera, D.; Balart, R. Development and optimization of renewable vinyl plastisol/wood flour composites exposed to ultraviolet radiation. *Mater. Des.* **2016**, *108*, 648–658. [CrossRef]

9. Ghofrani, M.; Pishan, S.; Mohammadi, M.R.; Omidi, H. A study on rice-husk/recycled high density polyethylene composites–their physical and mechanical properties. *Environ. Sci.* **2011**, *9*, 99–112.

10. Dimzoski, B.; Bogoeva-Gaceva, G.; Gentile, G.; Avella, M.; Grozdanov, A. Polypropylene-based eco-composites filled with agricultural rice hulls waste. *Chem. Biochem. Eng. Q.* **2009**, *23*, 225–230.

11. Prabu, V.A.; Johnson, R.D.J.; Amuthakkannan, P.; Manikandan, V. Usage of industrial wastes as particulate composite for environment management: Hardness, tensile and impact studies. *J. Environ. Chem. Eng.* **2017**, *5*, 1289–1301. [CrossRef]

12. Prabhakar, M.; Shah, A.U.R.; Rao, K.C.; Song, J.-I. Mechanical and thermal properties of epoxy composites reinforced with waste peanut shell powder as a bio-filler. *Fibers Polym.* **2015**, *16*, 1119–1124. [CrossRef]

13. Ikladious, N.; Shukry, N.; El-Kalyoubi, S.; Asaad, J.; Mansour, S.; Tawfik, S.; Abou-Zeid, R. Eco-friendly composites based on peanut shell powder/unsaturated polyester resin. *Proc. Inst. Mech. Eng. Part L J. Mater. Des. Appl.* **2019**, *233*, 955–964. [CrossRef]

14. Quiles-Carrillo, L.; Montanes, N.; Garcia-Garcia, D.; Carbonell-Verdu, A.; Balart, R.; Torres-Giner, S. Effect of different compatibilizers on injection-molded green composite pieces based on polylactide filled with almond shell flour. *Compos. Part B Eng.* **2018**, *147*, 76–85. [CrossRef]

15. Singh, V.; Bansal, G.; Agarwal, M.; Negi, P. Experimental determination of mechanical and physical properties of almond shell particles filled biocomposite in modified epoxy resin. *J. Mater. Sci. Eng.* **2016**, *5*. [CrossRef]

16. Liminana, P.; Garcia-Sanoguera, D.; Quiles-Carrillo, L.; Balart, R.; Montanes, N. Development and characterization of environmentally friendly composites from poly (butylene succinate)(PBS) and almond shell flour with different compatibilizers. *Compos. Part B Eng.* **2018**, *144*, 153–162. [CrossRef]

17. Barczewski, M.; Sałasińska, K.; Szulc, J. Application of sunflower husk, hazelnut shell and walnut shell as waste agricultural fillers for epoxy-based composites: A study into mechanical behavior related to structural and rheological properties. *Polym. Test.* **2019**, *75*, 1–11. [CrossRef]

18. Balart, J.; Montanes, N.; Fombuena, V.; Boronat, T.; Sánchez-Nacher, L. Disintegration in compost conditions and water uptake of green composites from poly (lactic acid) and hazelnut shell flour. *J. Polym. Environ.* **2018**, *26*, 701–715. [CrossRef]

19. Ameh, A.O.; Isa, M.T.; Sanusi, I. Effect of particle size and concentration on the mechanical properties of polyester/date palm seed particulate composites. *Leonardo Electron. J. Pract. Technol.* **2015**, *26*, 65–78.

20. Sharma, H.; Singh, I.; Misra, J.P. Mechanical and thermal behaviour of food waste (Citrus limetta peel) fillers–based novel epoxy composites. *Polym. Polym. Compos.* **2019**, *27*, 527–535. [CrossRef]

21. Garcia-Garcia, D.; Quiles-Carrillo, L.; Montanes, N.; Fombuena, V.; Balart, R. Manufacturing and Characterization of Composite Fibreboards with Posidonia oceanica Wastes with an Environmentally-Friendly Binder from Epoxy Resin. *Materials* **2018**, *11*, 35. [CrossRef] [PubMed]

22. Ferrero, B.; Fombuena, V.; Fenollar, O.; Boronat, T.; Balart, R. Development of natural fiber-reinforced plastics (NFRP) based on biobased polyethylene and waste fibers from Posidonia oceanica seaweed. *Polym. Compos.* **2015**, *36*, 1378–1385. [CrossRef]

23. Koutsomitopoulou, A.; Bénézet, J.; Bergeret, A.; Papanicolaou, G. Preparation and characterization of olive pit powder as a filler to PLA-matrix bio-composites. *Powder Technol.* **2014**, *255*, 10–16. [CrossRef]

24. Naghmouchi, I.; Espinach, F.X.; Mutjé, P.; Boufi, S. Polypropylene composites based on lignocellulosic fillers: How the filler morphology affects the composite properties. *Mater. Des. (1980–2015)* **2015**, *65*, 454–461. [CrossRef]

25. D'Amato, D.; Veijonaho, S.; Toppinen, A. Towards sustainability? Forest-based circular bioeconomy business models in Finnish SMEs. *For. Policy Econ.* **2020**, *110*, 101848. [CrossRef]

26. Capezza, A.J.; Lundman, M.; Olsson, R.T.; Newson, W.R.; Hedenqvist, M.S.; Johansson, E. Carboxylated wheat gluten proteins—A green solution for production of sustainable superabsorbent materials. *Biomacromolecules* **2020**, *21*, 1709–1719. [CrossRef]

27. Barczewski, M.; Mysiukiewicz, O.; Kloziński, A. Complex modification effect of linseed cake as an agricultural waste filler used in high density polyethylene composites. *Iran. Polym. J.* **2018**, *27*, 677–688. [CrossRef]

28. Food and Agriculture Organization. Available online: http://www.fao.org (accessed on 28 April 2020).

29. Zhang, Z.-S.; Wang, L.-J.; Li, D.; Jiao, S.-S.; Chen, X.D.; Mao, Z.-H. Ultrasound-assisted extraction of oil from flaxseed. *Sep. Purif. Technol.* **2008**, *62*, 192–198. [CrossRef]

30. Yasmeen, M.; Nisar, S.; Tavallali, V.; Khalid, T. A review of phytochemicals and uses of flaxseed. *Int. J. Chem. Biochem. Sci.* **2018**, *13*, 70–75.

31. Bekhit, A.E.-D.A.; Shavandi, A.; Jodjaja, T.; Birch, J.; Teh, S.; Ahmed, I.A.M.; Al-Juhaimi, F.Y.; Saeedi, P.; Bekhit, A.A. Flaxseed: Composition, detoxification, utilization, and opportunities. *Biocatal. Agric. Biotechnol.* **2018**, *13*, 129–152. [CrossRef]

32. Zhang, Z.-S.; Wang, L.-J.; Li, D.; Li, S.-J.; Özkan, N. Characteristics of flaxseed oil from two different flax plants. *Int. J. Food Prop.* **2011**, *14*, 1286–1296. [CrossRef]

33. Mannucci, A.; Castagna, A.; Santin, M.; Serra, A.; Mele, M.; Ranieri, A. Quality of flaxseed oil cake under different storage conditions. *LWT* **2019**, *104*, 84–90. [CrossRef]

34. Brison, L. Evaluation of the Effect of Nitrogen Fertilization and Tillage on the Yield and the Nutritional Profile of Flaxseed. Master's Thesis, Université catholique de Louvain, Ottignies-Louvain-la-Neuve, Belgium, 2019.

35. Wirkijowska, A.; Zarzycki, P.; Sobota, A.; Nawrocka, A.; Blicharz-Kania, A.; Andrejko, D. The possibility of using by-products from the flaxseed industry for functional bread production. *LWT* **2020**, *118*, 108860. [CrossRef]

36. Kolodziejczyk, P.; Ozimek, L.; Kozłowska, J. The application of flax and hemp seeds in food, animal feed and cosmetics production. In *Handbook of Natural Fibres*; Elsevier: Amsterdam, The Netherlands, 2012; pp. 329–366.

37. Chan, C.M.; Vandi, L.-J.; Pratt, S.; Halley, P.; Richardson, D.; Werker, A.; Laycock, B. Composites of wood and biodegradable thermoplastics: A review. *Polym. Rev.* **2018**, *58*, 444–494. [CrossRef]

38. España, J.; Samper, M.; Fages, E.; Sánchez-Nácher, L.; Balart, R. Investigation of the effect of different silane coupling agents on mechanical performance of basalt fiber composite laminates with biobased epoxy matrices. *Polym. Compos.* **2013**, *34*, 376–381. [CrossRef]

39. Bertomeu, D.; García-Sanoguera, D.; Fenollar, O.; Boronat, T.; Balart, R. Use of eco-friendly epoxy resins from renewable resources as potential substitutes of petrochemical epoxy resins for ambient cured composites with flax reinforcements. *Polym. Compos.* **2012**, *33*, 683–692. [CrossRef]

40. Samper, M.; Fombuena, V.; Boronat, T.; García-Sanoguera, D.; Balart, R. Thermal and mechanical characterization of epoxy resins (ELO and ESO) cured with anhydrides. *J. Am. Oil Chem. Soc.* **2012**, *89*, 1521–1528. [CrossRef]

41. Fombuena, V.; Samper, M.; Sanchez-Nacher, L. Study of the properties of thermoset materials derived from epoxidized soybean oil and protein fillers. *J. Am. Oil Chem. Soc.* **2013**, *90*, 449–457. [CrossRef]

42. Carbonell-Verdu, A.; Bernardi, L.; Garcia-Garcia, D.; Sanchez-Nacher, L.; Balart, R. Development of environmentally friendly composite matrices from epoxidized cottonseed oil. *Eur. Polym. J.* **2015**, *63*, 1–10. [CrossRef]

43. Anusic, A.; Resch-Fauster, K.; Mahendran, A.R.; Wuzella, G. Anhydride Cured Bio-Based Epoxy Resin: Effect of Moisture on Thermal and Mechanical Properties. *Macromol. Mater. Eng.* **2019**, *304*, 1900031. [CrossRef]

44. Quiles-Carrillo, L.; Duart, S.; Montanes, N.; Torres-Giner, S.; Balart, R. Enhancement of the mechanical and thermal properties of injection-molded polylactide parts by the addition of acrylated epoxidized soybean oil. *Mater. Des.* **2018**, *140*, 54–63. [CrossRef]

45. Fenollar, O.; Sanchez-Nacher, L.; Garcia-Sanoguera, D.; López, J.; Balart, R. The effect of the curing time and temperature on final properties of flexible PVC with an epoxidized fatty acid ester as natural-based plasticizer. *J. Mater. Sci.* **2009**, *44*, 3702–3711. [CrossRef]

46. Liu, X.; Huang, W.; Jiang, Y.; Zhu, J.; Zhang, C. Preparation of a bio-based epoxy with comparable properties to those of petroleum-based counterparts. *Express Polym. Lett.* **2012**, *6*, 293–298. [CrossRef]

47. Niedermann, P.; Szebényi, G.; Toldy, A. Characterization of high glass transition temperature sugar-based epoxy resin composites with jute and carbon fibre reinforcement. *Compos. Sci. Technol.* **2015**, *117*, 62–68. [CrossRef]

48. Niedermann, P.; Szebényi, G.; Toldy, A. Effect of epoxidized soybean oil on curing, rheological, mechanical and thermal properties of aromatic and aliphatic epoxy resins. *J. Polym. Environ.* **2014**, *22*, 525–536. [CrossRef]

49. Wu, Y.; Wang, Y.; Yang, F.; Wang, J.; Wang, X. Study on the Properties of Transparent Bamboo Prepared by Epoxy Resin Impregnation. *Polymers* **2020**, *12*, 863. [CrossRef]

50. Salasinska, K.; Mizera, K.; Barczewski, M.; Borucka, M.; Gloc, M.; Celiński, M.; Gajek, A. The influence of degree of fragmentation of Pinus sibirica on flammability, thermal and thermomechanical behavior of the epoxy-composites. *Polym. Test.* **2019**, *79*, 106036. [CrossRef]

51. Kumar, R.; Kumar, K.; Bhowmik, S. Mechanical characterization and quantification of tensile, fracture and viscoelastic characteristics of wood filler reinforced epoxy composite. *Wood Sci. Technol.* **2018**, *52*, 677–699. [CrossRef]

52. Stabik, J.; Chomiak, M. Graded epoxy-hard coal composites: Analysis of filler particle distribution in the epoxy matrix. *J. Compos. Mater.* **2016**, *50*, 3663–3677. [CrossRef]

53. Lascano, D.; Quiles-Carrillo, L.; Torres-Giner, S.; Boronat, T.; Montanes, N. Optimization of the curing and post-curing conditions for the manufacturing of partially bio-based epoxy resins with improved toughness. *Polymers* **2019**, *11*, 1354. [CrossRef]

54. Agüero, Á.; Lascano, D.; Garcia-Sanoguera, D.; Fenollar, O.; Torres-Giner, S. Valorization of Linen Processing By-Products for the Development of Injection-Molded Green Composite Pieces of Polylactide with Improved Performance. *Sustainability* **2020**, *12*, 652. [CrossRef]

55. Bledzki, A.K.; Mamun, A.A.; Volk, J. Barley husk and coconut shell reinforced polypropylene composites: The effect of fibre physical, chemical and surface properties. *Compos. Sci. Technol.* **2010**, *70*, 840–846. [CrossRef]

56. Salasinska, K.; Barczewski, M.; Górny, R.; Kloziński, A. Evaluation of highly filled epoxy composites modified with walnut shell waste filler. *Polym. Bull.* **2018**, *75*, 2511–2528. [CrossRef]

57. Kwon, H.-J.; Sunthornvarabhas, J.; Park, J.-W.; Lee, J.-H.; Kim, H.-J.; Piyachomkwan, K.; Sriroth, K.; Cho, D. Tensile properties of kenaf fiber and corn husk flour reinforced poly (lactic acid) hybrid bio-composites: Role of aspect ratio of natural fibers. *Compos. Part B Eng.* **2014**, *56*, 232–237. [CrossRef]

58. Bisht, N.; Gope, P.C. Mechanical properties of rice husk flour reinforced epoxy bio-composite. *Int. J. Eng. Res. Appl.* **2015**, *5*, 123128.

59. Novowood. Available online: https://www.novowood.it/en/download-technical-sheet-wpc_39c7.html (accessed on 18 May 2020).

60. Jeluplast. Available online: https://www.jeluplast.com/wp-content/uploads/2013/09/WPC-PE-H70-800-03.pdf (accessed on 18 May 2020).

61. García-García, D.; Carbonell, A.; Samper, M.; García-Sanoguera, D.; Balart, R. Green composites based on polypropylene matrix and hydrophobized spend coffee ground (SCG) powder. *Compos. Part B Eng.* **2015**, *78*, 256–265. [CrossRef]

62. Yussuf, A.; Massoumi, I.; Hassan, A. Comparison of polylactic acid/kenaf and polylactic acid/rise husk composites: The influence of the natural fibers on the mechanical, thermal and biodegradability properties. *J. Polym. Environ.* **2010**, *18*, 422–429. [CrossRef]

63. Raju, G.; Kumarappa, S. Experimental study on mechanical and thermal properties of epoxy composites filled with agricultural residue. *Polym. Renew. Resour.* **2012**, *3*, 117–138. [CrossRef]

64. Chen, W.-H.; Kuo, P.-C. A study on torrefaction of various biomass materials and its impact on lignocellulosic structure simulated by a thermogravimetry. *Energy* **2010**, *35*, 2580–2586. [CrossRef]

65. Moriana, R.; Vilaplana, F.; Ek, M. Forest residues as renewable resources for bio-based polymeric materials and bioenergy: Chemical composition, structure and thermal properties. *Cellulose* **2015**, *22*, 3409–3423. [CrossRef]

66. Hussain, S.; Anjum, F.; Butt, M.; Sheikh, M. Chemical composition and functional properties of flaxseed (*Linum usitatissimum*) flour. *Sarhad J. Agric.* **2008**, *24*, 649–653.

67. Sengupta, S.; Maity, P.; Ray, D.; Mukhopadhyay, A. Stearic acid as coupling agent in fly ash reinforced recycled polypropylene matrix composites: Structural, mechanical, and thermal characterizations. *J. Appl. Polym. Sci.* **2013**, *130*, 1996–2004. [CrossRef]

68. Mysiukiewicz, O.; Barczewski, M. Utilization of linseed cake as a postagricultural functional filler for poly (lactic acid) green composites. *J. Appl. Polym. Sci.* **2019**, *136*, 47152. [CrossRef]

69. Liu, R.; Wang, J.; He, Q.; Zong, L.; Jian, X. Interaction and properties of epoxy-amine system modified with poly (phthalazinone ether nitrile ketone). *J. Appl. Polym. Sci.* **2016**, *133*. [CrossRef]

70. Balart, J.; García-Sanoguera, D.; Balart, R.; Boronat, T.; Sánchez-Nacher, L. Manufacturing and properties of biobased thermoplastic composites from poly (lactid acid) and hazelnut shell wastes. *Polym. Compos.* **2018**, *39*, 848–857. [CrossRef]

71. Balart, J.; Fombuena, V.; Fenollar, O.; Boronat, T.; Sánchez-Nacher, L. Processing and characterization of high environmental efficiency composites based on PLA and hazelnut shell flour (HSF) with biobased plasticizers derived from epoxidized linseed oil (ELO). *Compos. Part B Eng.* **2016**, *86*, 168–177. [CrossRef]

72. Liminana, P.; Quiles-Carrillo, L.; Boronat, T.; Balart, R.; Montanes, N. The Effect of Varying Almond Shell Flour (ASF) Loading in Composites with Poly (Butylene Succinate (PBS) Matrix Compatibilized with Maleinized Linseed Oil (MLO). *Materials* **2018**, *11*, 2179. [CrossRef]

73. Reixach, R.; Puig, J.; Méndez, J.A.; Gironès, J.; Espinach, F.X.; Arbat, G.; Mutjé, P. Orange wood fiber reinforced polypropylene composites: Thermal properties. *Bioresources* **2015**, *10*. [CrossRef]

74. Akil, H.M.; Cheng, L.W.; Ishak, Z.M.; Bakar, A.A.; Rahman, M.A. Water absorption study on pultruded jute fibre reinforced unsaturated polyester composites. *Compos. Sci. Technol.* **2009**, *69*, 1942–1948. [CrossRef]

75. Ferrero, B.; Boronat, T.; Moriana, R.; Fenollar, O.; Balart, R. Green composites based on wheat gluten matrix and posidonia oceanica waste fibers as reinforcements. *Polym. Compos.* **2013**, *34*, 1663–1669. [CrossRef]

76. Alander, B.; Capezza, A.; Wu, Q.; Johansson, E.; Olsson, R.T.; Hedenqvist, M. A facile way of making inexpensive rigid and soft protein biofoams with rapid liquid absorption. *Ind. Crops Prod.* **2018**, *119*, 41–48. [CrossRef]

77. Ben Daly, H.; Ben Brahim, H.; Hfaied, N.; Harchay, M.; Boukhili, R. Investigation of water absorption in pultruded composites containing fillers and low profile additives. *Polym. Compos.* **2007**, *28*, 355–364. [CrossRef]

78. Udhayasankar, R.; Kathikeyan, B. Preparation and properties of cashew nut shell liquid-Based composite reinforced by coconut shell particles. *Surf. Rev. Lett.* **2019**, *26*, 1850174. [CrossRef]

79. Naghmouchi, I.; Mutjé, P.; Boufi, S. Polyvinyl chloride composites filled with olive stone flour: Mechanical, thermal, and water absorption properties. *J. Appl. Polym. Sci.* **2014**, *131*. [CrossRef]

80. Shehu, U.; Aponbiede, O.; Ause, T.; Obiodunukwe, E. Effect of particle size on the properties of polyester/palm kernel shell (PKS) particulate composites. *J. Mater. Environ. Sci.* **2014**, *5*, 366–373.

81. Thirmizir, M.A.; Ishak, Z.M.; Taib, R.M.; Sudin, R.; Leong, Y. Mechanical, water absorption and dimensional stability studies of kenaf bast fibre-filled poly (butylene succinate) composites. *Polym. Plast. Technol. Eng.* **2011**, *50*, 339–348. [CrossRef]

82. Zabihzadeh, S.M.; Omidvar, A.; Marandi, M.A.B.; Dastoorian, F.; Mirmehdi, S.M. Effect of filler loading on physical and flexural properties of rapeseed stem/PP composites. *BioResources* **2011**, *6*, 1475–1483.

83. Ishak, Z.M.; Yow, B.; Ng, B.; Khalil, H.A.; Rozman, H. Hygrothermal aging and tensile behavior of injection-molded rice husk-filled polypropylene composites. *J. Appl. Polym. Sci.* **2001**, *81*, 742–753. [CrossRef]

84. Najafi, A.; Khademi-Eslam, H. Lignocellulosic filler/recycled HDPE composites: Effect of filler type on physical and flexural properties. *BioResources* **2011**, *6*, 2411–2424.

85. Sapuan, S.; Harun, N.; Abbas, K. Design and fabrication of a multipurpose table using a composite of epoxy and banana pseudostem fibres. *J. Trop. Agric.* **2008**, *45*, 66–68.

86. Sapuan, S.; Maleque, M. Design and fabrication of natural woven fabric reinforced epoxy composite for household telephone stand. *Mater. Des.* **2005**, *26*, 65–71. [CrossRef]